JPET Fast Forward. Published on June 28, 2019 as DOI: 10.1124/jpet.118.255851
This article has not been copyedited and formatted. The final version may differ from this version.

JPET #255851

Target Engagement of a Phosphodiesterase 2 (PDE2A) Inhibitor Affecting Long-Term Memory in the Rat

Guibao Gu, Trevor Scott, Yingzhuo Yan, Noelle Warren, Adia Zhang, Ali Tabatabaei, Hao Xu, Kathleen Aertgeerts, Laurent Gomez, Andrew Morse, Yu-Wen Li, J. Guy Breitenbucher, Eben Massari, Jeffrey Vivian, Anne Danks

Author affiliations:

Department of Preclinical Research (G. G., T. S., N.W., A.T., Y. W. L., A. M., J. V., A.D.), Department of Chemistry Manufacturing and Control (A. Z.), Department of Biology (Y. Y., E. M.), Department of Structural Biology (H. X., K. A.), Department of Medicinal Chemistry (L. G., G. B.), Dart NeuroScience, LLC, San Diego, California, USA 92131

JPET Fast Forward. Published on June 28, 2019 as DOI: 10.1124/jpet.118.255851
This article has not been copyedited and formatted. The final version may differ from this version.

JPET #255851

Running title: PDE2A Target Occupancy by PDE2A Inhibitor

Corresponding Author: Guibao Gu, M.D., Ph.D.

12278 Scripps Summit Drive,

San Diego, CA 92131

Work Tel: 858-245-9018

Email: gug726@yahoo.com

No. of text pages: (including title pages): 37

No. of tables: 1

No. of figures: 9

No. of references: 51

No. of words in Abstract: 242

No. of words in Introduction: 750

No. of words in Discussion: 1352

Abbreviations:

PDE2A, Phosphodiesterase 2; cGMP; cAMP; NMDA, N-methyl-d-Aspartate; MCI, Mild cognitive Impairment; AD, Alzheimer's Disease; CREB, cAMP response element binding protein

Abstract

Inhibition of phosphodiesterase 2A (PDE2A) has been proposed as a potential approach to enhance cognitive functioning and memory through boosting intracellular cGMP/cAMP and enhancing neuroplasticity in memory-related circuitry. Previous preclinical studies demonstrated that PDE2A inhibitors could reverse NMDA receptor antagonist MK801 or ketamine-induced memory deficit. Here we report that the potent and selective PDE2A inhibitor PF-05180999 enhances long-term memory in a contextual fear conditioning model in the rat at the oral dose of 0.3 mg/kg. Target engagement at this efficacious dose was explored using *in vivo* autoradiography. Converse to the results of a decrease of PDE2A binding (target occupancy) by the PDE2A inhibitor, a paradoxical, up to 40% increase in PDE2A binding was detected. However, a typical target occupancy curve could be generated by PF-05180999 at much higher doses. *In vitro* experiments using recombinant PDE2A protein or rat brain homogenate that contains native PDE2A protein demonstrated that increased cGMP after initial PDE2A inhibition could be responsible for the activation of PDE2A enzyme via an allosteric binding to the GAF-B domain, leading to a positive cooperativity of the dormant PDE2A enzymes. Our results suggest that when evaluating target engagement of PDE2A inhibitors for memory disorder in clinical setting with occupancy assays, the efficacious dose may not fall on the typical receptor/target curve. On the contrary, an increase of PDE2A tracer binding is likely seen. Our results also suggest that when evaluating target occupancy of enzymes, potential regulation of enzyme activities should be considered.

Introduction

Cognitive decline is one of the most frequent health complaints of healthy individuals as they age, and even more pronounced in diagnosed neurocognitive disorders such as Alzheimer's disease (AD), dementia with Lewy body, or frontotemporal dementia (Petersen et al., 1999; Fleischman et al., 2004; Budson and Price, 2005; American Psychiatric Association, 2013). Physiologically, long-term memory relies on the plastic enhancement of specific neural circuitry (Kandel et al., 2014; Poo et al., 2016). The neuronal plasticity requires de novo protein synthesis and the activation of cyclic adenosine monophosphate (cAMP) response element binding protein (CREB) transcription factor was found to play a pivotal role in this process (Silva et al., 1998; Tully et al., 2003; Chen et al., 2010; Kandel, 2012). CREB is a transcription factor (Brindle and Montminy, 1992). Phosphorylation of CREB promotes the expression of genes with upstream cAMP response elements (Ginty et al., 1993; Gu et al., 1996). Several intracellular signaling pathways are known to activate CREB, and cAMP and Ca^{2+} are perhaps the most important regulators (Montminy et al., 1990; Soderling, 1999; West et al., 2001). Similarly, intracellular cyclic guanosine monophosphate (cGMP) can also activate CREB via cGMP-dependent protein kinase (Lu and Ding, 1999; Paul et al., 2010). Therefore, it is conceivable that managing intracellular cAMP, and/or cGMP levels would help manipulate CREB phosphorylation and enhance neural circuitry plasticity (Teich et al., 2015).

Levels of intracellular cAMP and/or cGMP are regulated by phosphodiesterases (PDEs) through hydrolysis to AMP and/or GMP. A family with 11 members, each PDE subtype

has multiple isoforms and splice variants (Conti and Beavo, 2007). PDE members are categorized by their catalytic domain selectivity and the properties of their regulatory domains (Schmidt, 2010; Conti and Richter, 2014). As a cGMP-stimulated cyclic nucleotide phosphodiesterase (Martins et al., 1982), PDE2A hydrolyzes both cAMP and cGMP, and possesses an allosteric GAF (cGMP activated PDEs, adenylyl cyclase, and Fh1A)-B domain that preferentially binds cGMP (Stroop and Beavo, 1991; Martinez et al., 2002; Wu et al., 2004; Pandit et al., 2009). Via a positive cooperativity mechanism, cGMP binding to the GAF domain causes a conformational change of the linker region between the catalytic and the regulatory domains of enzyme, swings the H-loops out, opens the access of the substrate and thereby upregulates the hydrolytic activity of PDE2A (Pandit et al., 2009).

The high abundance and preferential expression in the brain indicates that PDE2A could serve as a suitable target for pharmacological intervention for memory disorders. PDE2A is highly expressed in brain regions that are important for cognitive functions, including the cerebral cortex, the hippocampus, and the striatum (Stephenson et al., 2012; Kelly et al., 2014). In *in vitro* and *in vivo* animal studies, PDE2A-selective inhibitors enhanced long-term potentiation (LTP) and improved the performance of multiple memory tasks (Boess et al., 2004; Domek-Lopacinska and Strosznajder, 2008; Helal et al., 2018; Nakashima et al., 2018).

Critical to the advancement of PDE2A inhibitor drugs in clinic is the identification and validation of specific biomarkers of drug action in the CNS. Recently PF-05270430

(Chen et al., 2016) was reported to be a useful PET ligand. The utility of PDE2A PET ligands depends on the establishment of a defined occupancy/efficacy relationship with the desired pharmacological effect. PDE2A inhibitor TAK-915 reversed MK-801 induced episodic memory deficits at an oral dose of 3 and 10 mg/kg (but not 1 mg/kg), which corresponded well with the dose that elevated hippocampal cGMP levels (Occupancy was reported to be about 46% and 63% at these doses) (Mikami et al., 2017a). However, TAK-915 significantly enhanced performance in the rat novel object recognition (NOR) study (Mikami et al., 2017b) at a dose of 0.1 mg/kg, presumably at an occupancy far lower than 46%. Similarly, another PDE2A inhibitor PF-05180999 demonstrated reversal of ketamine-induced working memory deficits in rats at doses of 0.1-0.32 mg/kg s.c., corresponding to “several fold less than 50% occupancy” (Helal et al., 2018). The phenomenon of efficacy in rodent memory models at very low occupancy was a common observation in our PDE2A drug discovery efforts (unpublished observation).

In evaluating PDE2A target occupancy by PDE2A inhibitors, the positive cooperativity of the enzyme should be considered. Since the doses of the PDE2A inhibitor required to reverse chemical-challenged cognitive deficits were relatively high (Mikami et al., 2017a; Helal et al., 2018), this positive cooperativity might have been masked. In the current study, we used a non-chemically challenged long-term memory retention model and *in vivo* autoradiography to investigate the target engagement of a potent and selective PDE2A inhibitor PF-05180999 at the low efficacious doses.

JPET Fast Forward. Published on June 28, 2019 as DOI: 10.1124/jpet.118.255851
This article has not been copyedited and formatted. The final version may differ from this version.

Materials and Methods

Materials

NIR Video Fear Conditioning System – Contextual Package (Med Associates, Inc., cat# MED-VFC2-SCT-R)

350-450gram male CD rats (Charles River)

Rat whole brain membranes (0.6 mg/mL)

^{3}H-PF-05270430 (Moravek)

96-well V-bottom dilution plates (Costar, cat# 29444-102)

96-well masterblock 0.5mL V-bottom assay plate (Greiner, cat# 78620)

96-well unifilter-GF/C filter plates (Perkin Elmer, cat# 6005174)

MicroScint-20 (Perkin Elmer, cat# 6013621)

Brandel Harvester (model # MWXRI-96TI)

2450 Micro Plate Reader (Perkin Elmer)

Omni Prep multi sample homogenizer (Kennesaw, GA)

Cryostat (CM-1950, Leica Microsystems)

Liquid Scintillation counter (Model LS6500, Beckman Coulter, Inc.)

75-100gram jugular vein-cannulated male CD rats (Charles River)

Plexiglass rat restrainer (Braintree Scientific, Inc.)

Beta-imager (Biospace Lab)

Methods

Animals

The protocols performed in the present rodent studies were approved by the Institutional Animal Use and Care Committee of Dart NeuroScience LLC., in accordance with the guidelines of the National Institutes of Health and the United States Department of Agriculture for the care and use of laboratory animals. Male CD rats, naïve or jugular vein-cannulated, weighing from 100 to 450 grams, were obtained from Charles River Laboratories (Hollister, CA) and housed in cages on a 12h light/dark cycle. Food and water were available ad libitum.

Drugs

Drugs used included PF-05180999 (4-(1-Azetidinyl)-7-methyl-5-[1-methyl-5-[5-(trifluoromethyl)-2-pyridinyl]-1*H*-pyrazol-4-yl]-imidazo[5,1-*f*][1,2,4]triazine, PDE2A IC_{50} = 1.6 nM, >56250-fold selectivity of PDE2A over PDE1B1, PDE3A1, PDE4D3, PDE5A1, and Bovine PDE6, 26969-fold over PDE7B, >56250-fold over PDE8B, PDE9A1, 2030-fold over PDE10A, and 50090-fold over PDE11A4 (Helal, et al., 2018), made by Dart NeuroScience, LLC., San Diego, CA), and ^{3}H-PF-05270430 (4-(3-fluoroazetidin-1-yl)-7-methyl-5-(1-methyl-5-(4-(trifluoromethyl)phenyl)-1H-pyrazol-4-yl)imidazo[1,5-f][1,2,4]triazine, PDE2A IC_{50} = 0.53 nM, >56604-fold selectivity for PDE2A over PDE1B, and >56604-fold over PDE3A, PDE4D, 49057-fold over PDE5A, >18868-fold over PDE6A, 22642-fold over PDE7B, >18868-fold over PDE8B, PDE9A, 7358-fold over PDE10A and >18868-fold over PDE11 (Zhang et al., 2013), made by Dart NeuroScience, LLC., San Diego, CA and Moravek Biochemicals (Brea, CA). PF-05180999 was freshly prepared in 10:40:50 or 10:60:30 N-Methyl-2-Pyrrolidone (NMP):

JPET Fast Forward. Published on June 28, 2019 as DOI: 10.1124/jpet.118.255851
This article has not been copyedited and formatted. The final version may differ from this version.

Polyethylene Glycol (PEG)-400:H2O solution. ^{3}H-PF-05270430 was freshly prepared in a solution of 50:30:20 PEG-400:H2O:Ethanol.

Contextual fear conditioning task (cFC)

The cFC task was performed in a conditioning chamber placed in a sound-attenuating box (Med Associates Inc, Vermont, USA) during the light phase of the cycle. CD male rats, weighing from 350 to 450 grams, were doubly housed in the holding room for 2 weeks prior to training/test. One hour after receiving oral dose of vehicle (10:40:50 NMP:PEG400:H2O) or PF-05180999 (synthesized by the Department of Chemistry, Dart Neuroscience, LLC) at the doses ranging from 0.03 to 1 mg/kg (2 mL/kg), all rats were trained and tested in the conditioning chambers equipped with a stainless-steel grid floor through which footshocks are delivered. Training consisted of placing the rats in the chamber and after a 120s baseline delivering two electrical footshocks (2s duration; 0.4 mA) separated by a 60s inter-trial interval. The two shocks serve as the aversive unconditioned stimulus (US) to induce a weak memory. Thirty seconds after the final shock, rats were removed from the chamber and returned to the home cage. Long-term memory was assessed 24h after training by placing the rats into the chambers with the same training context and calculating the percentage of time spent freezing during 3 min without footshock. Freezing behavior was defined as the complete lack of movement, except for respiration, and was measured automatically using Video Freeze software.

Radioactive Tracer Labeling

PF-05270430 was labeled with tritium as the PDE2A ligand by Moravek Biochemicals. The ligand was radiolabeled from the cold compound synthesized by the Department of Chemistry, Dart Neuroscience, LLC, by a direct exchange of hydrogen atoms with its isotope tritium using the Crabtree's catalyst and tritium gas under anhydrous conditions. The reaction was stirred at room temperature for 24h. The crude product was dissolved in ethanol and evaporated to dryness three times. The radioligand was purified on a HPLC-C18 Capcell Pak column, mobile phase 45% acetonitrile, 0.1% trifluoroacetic acid (TFA), Ultraviolet 254 nm, flow rate 6 mL/min. A radiochemical purity of over 99.3% and the specific activity of over 87 Ci/mmol were achieved. The tritium tracer was then packaged in 100% ethanol and stored at -20 ^{o}C before use.

Rat Brain Membrane Preparation

Naïve rats were deeply anesthetized with isoflurane vapor in a Bell-jar and brains quickly removed from the skull and immediately frozen in isopentane bath chilled with dry ice. Frozen brains were then stored in -80 ^{o}C freezer before use. During membrane preparation, whole flash-frozen rat brains were thawed on ice, split into two halves down the midline. Each half was added to a 15 mL centrifugation tube containing 7 mL of ice-cold assay buffer (50mM Tris HCL, 1mM $MgCl_2$, 1mM $CaCl_2$, 2mM KCl, pH 7.4). Brains were further homogenized on ice using the Omni Prep multi sample homogenizer at 14,000 RPM for 90s. After homogenization, samples were centrifuged at 15000g for 30 min. Supernatant was discarded and pellet re-suspended in 7 mL ice cold assay buffer. Re-suspended membranes were then pooled together and kept on ice. Following the

JPET Fast Forward. Published on June 28, 2019 as DOI: 10.1124/jpet.118.255851
This article has not been copyedited and formatted. The final version may differ from this version.

determination of the total protein concentration using the BCA method, one milliliter aliquots were made, frozen on dry ice, and stored at -80 ^{o}C before use.

K_d and B_{max} Determination

The *K_d* (dissociation constant at equilibrium) and B_{max} (maximum number of binding sites) values of the radio-labeled tracer were measured with rat brain homogenate. Binding reactions were set up in a 96 well assay plate (156 µg/well total protein). Various concentrations of ^{3}H-radioligand in the absence (for total binding) or presence (for nonspecific binding) of 10 µM unlabeled form of the ligand were incubated with rat brain homogenate protein at room temperature for 2h. The assay solutions were then filtered using a Brandel Harvester onto a 96 well GF/C filter plate. The filter plate was washed using 2 L of wash buffer (50mM Tris HCL, 1mM $MgCl_2$, pH 7.4). After drying, each well of the filter was added to 50 mL of Microscint-20 scintillation fluid and the plate counted with a MicroBeta counter (Perkin Elmer). The specific binding was calculated by subtracting the nonspecific binding from the total binding for each concentration used in the assay and the data was fit to a one-site specific binding curve using GraphPad Prism software. B_{max} was calculated using GraphPad quick calcs based on the specific activity of the radioligand, microbeta counter efficiency (43%), and total protein concentration (156 µg/well).

K_i Assay

An *in vitro* Ki assay was performed to examine displacement of the radiolabeled PDE2A tracer by PF-05180999. Compound PF-05180999 was first serially diluted ranging from 0.05 nM to 50 µM in duplicate with 0.5% Dimethyl sulfoxide (DMSO)/assay buffer in a

JPET Fast Forward. Published on June 28, 2019 as DOI: 10.1124/jpet.118.255851
This article has not been copyedited and formatted. The final version may differ from this version.

96-well 0.5 mL v-bottom assay plate. Total binding or nonspecific binding controls were placed in the wells by skipping the test article or adding 10 μM of the unlabeled form of the radioligand in 0.5% DMSO/assay buffer. ^{3}H-PF-05270430 at the concentration of K_d and 156 μg/well total protein of the membrane prep were added into each well and incubate for 2h at room temperature with slow agitation. The assay solutions were harvested and the counts measured following procedures described above. The specific binding was calculated by subtracting the nonspecific binding from the total binding for each concentration used in the assay. The IC_{50} value was determined and the 11-point inhibition curve plotted using GraphPad Prism software. The IC_{50} values were converted to Ki value according to Chang Prusoff Equation $Ki = IC_{50}/(1+[S]/K_d)$, where $[S] = K_d$.

In vivo PDE2A Occupancy

An *in vivo* autoradiography method was used to explore PDE2A target occupancy in the rat by PF-05180999. The radioactive tracer ^{3}H-PF-05270430 was first characterized in live animal by *i.v.* dosing into jugular vein-cannulated CD rats weighing from 100 to 150 grams to identify proper dose and time point of the tracer, at which the radioactivity of region of interest (ROI) reached 0.5 to 1.0 cpm/mm^2 and the best signal/noise (ROI/REF (reference region)) ratio is achieved. In *in vivo* occupancy experiments, 0.03 to 150 mg/kg PF-05180999 or vehicle (10:40:50 or 10:60:30 NMP:PEG400:H2O) were orally dosed. Fifty minutes later, approximately 300 μL blood was drawn from the jugular cannula and collected in tubes with lithium heparin gel barrier (Terumo Corporation, Somerset, NJ). Plasma was prepared by centrifugation for compound concentration analysis. Immediately following plasma collection, rats then received a total volume of

600 µL tritiated tracer (0.5 µCi/g or 1 µCi/g per body weight, in 50% PEG400, 20% ethanol, and 30% H_2O vehicle) into the jugular vein, followed by 500 µL saline flush. Injections lasted at least for 30s to avoid circulatory failure. Ten minutes later, following anesthesia with isoflurane in a Bell jar, each rat was decapitated, 500 µL of trunk blood was collected in tubes with lithium heparin gel barrier, and plasma isolated by centrifugation for radioactivity quantitation. Brain tissue from each rat was quickly removed, frozen in dry ice-chilled isopentane, and stored at -80°C before further processing. Sagittal brain sections were cut at 20 um with a Leica CM1950 cryostat and mounted on Superfrost plus slides. After drying at room temperature, slides were imaged with a Beta-imager (Biospace Lab, Paris, France). Acquired images were then analyzed with M3Vison software. Occupancy values were calculated as: *%Occupancy* = *(Vehicle Binding – Drug Binding)/Vehicle Binding* x *100.* The non-displaceable signals in the REF referred as the nonspecific binding were subtracted from all values prior to the calculation. Negative values were excluded in occupancy-exposure curve plotting.

In vitro recombinant PDE2A Protein binding

To elucidate the role of cGMP activation produced by PDE2A inhibition, an *in vitro* binding assay was developed using a recombinant PDE2A protein. The cDNA corresponding to residues 215-900 of human PDE2A3 (UniProt entry:O00408) followed by a tobacco etch virus (TEV) protease cleavage site, a 10x polyhistidine tag and a FLAG tag was synthesized, codon optimized (DNA2.0, Neward, CA, USA) and subcloned into a modified pFastbac1 vector (Thermo Fisher Scientific, Waltham, MA,

USA). High titer recombinant baculoviruses (>10^8 infective viral particles per milliliter) were generated using the Bac-to-Bac Baculovirus Expression System (Thermo Fisher Scientific) and were used to infect Spodoptera Frugiperda 9 (Sf9) insect cells at a density of 2×10^6 cells/mL with high titer viral stock at a multiplicity of infection of 5. Infected cells were grown at 27°C for 48-96h prior to being harvested, and the cell pellets were stored at -80°C. 2.5L of frozen cells were broken into small pieces and resuspended into 200mL lysis buffer (50mM Tris pH 7.5; 800 mM NaCl; 5% glycerol; 0.25 mM tris(2-carboxyethyl)phosphine (TCEP) and 1 tablet of a protease inhibitor cocktail (Roche)). After centrifugation, the sample was passed through a cheese cloth. 20ul of Universal Nuclease (Thermo Fisher Scientific, Waltham, MA, USA) and 9mL of a Probond Ni Resin (Thermo Fisher Scientific, Waltham, MA, USA) were added to the sample and incubated for 3h. Gravity-assisted flow was used to wash the resin with 300mL of 50mM Tris pH 7.5; 600 mM NaCl; 5% glycerol; 20mM imidazole. The protein was then eluted with 7 column volumes (~25mL) of 50mM Tris pH 7.5; 600 mM NaCl; 5% glycerol and 300mM imidazole. The protein was then further purified by size-exclusion chromatography using a Superdex 200 column (GE Healthcare Life Sciences, USA) with a flow of 1mL/min using a buffer containing 25mM Hepes pH 7.5; 50mM NaCl and 0.25mM TCEP. The fractions with the desired retention time were pooled. The final protein concentration was 0.56 mg/mL.

cGMP regulation of PDE2A ligand binding

PDE2A (215-900) protein (1 nM) was incubated with 10 nM ^{3}H-PF-05270430 and various concentrations of cGMP (0-100 mM) in assay buffer (25 mM Tris HCl, PH7.4, 5

JPET Fast Forward. Published on June 28, 2019 as DOI: 10.1124/jpet.118.255851
This article has not been copyedited and formatted. The final version may differ from this version.

mM $MgCl_2$, 0.2% BSA, 0.5 mM 1,4-dithiothreitol (DTT), and 0.05% Tween-20) at room temperature for 1h in 96-well non-binding surface (NBS) plates (Corning). PDE2A was subsequently captured by addition of a 1:4 dilution of ANTI-FLAG® M2 Affinity Gel (Sigma) prepared in assay buffer, incubated for additional 1h at room temperature and then transferred to glass fiber filter plates (UniFilter-96 GF/C Microplate, Perkin Elmer Life Sciences, Boston, MA, U.S.A.) pre-soaked in a 0.5% polyethyleneimine solution. Filters were washed six times with wash buffer (50mM Tris pH 7.5, 5 mM $MgCl_2$, 1 mM EDTA) using a Brandel harvester and the remaining radioactivity was quantified using a Microbeta Trilux counter (Perkin Elmer Life Sciences) using Microscint-20 (PerkinElmer Life Sciences). Non-specific binding was determined in the presence of 10 μM PF-05270430 and 100 μM cGMP.

K_d and B_{max} Determination in the presence or absence of cGMP

In a 96-well NBS plate, 1 nM of PDE2A (215-900) protein and various concentrations of ^{3}H-PF-05270430 (0 – 200 nM) were incubated in assay buffer (25 mM Tris HCl, pH 7.4, 5 mM $MgCl_2$, 0.2% BSA, 0.5 mM DTT, and 0.05% Tween-20) or assay buffer containing 30 μM cGMP at room temperature for 1h. PDE2A protein capture, washing and counting of the remaining radioactivity were performed as described above. K_d and B_{max} values were determined in Prism 7 (GraphPad, Inc.) by fitting data using a one-site model.

In vitro Native PDE2A Protein Binding in the absence or presence of cGMP

In vitro PDE2A binding in the absence or presence of cGMP PDE2A was examined with native PDE2A protein with rat brain homogenate, as prepared above. 0.1 mg/mL protein

JPET Fast Forward. Published on June 28, 2019 as DOI: 10.1124/jpet.118.255851
This article has not been copyedited and formatted. The final version may differ from this version.

was incubated with 0.5 nM ^{3}H-PF-05270430 and various concentrations of cGMP (0-10 mM) in assay buffer (50 mM Tris HCl, 1 mM $MgCl_2$, 1 mM $CaCl_2$, 2 mM KCl, pH 7.4) at room temperature for 5 min in 96-well NBS plates (Corning) in the presence of 10 μM PDE10 inhibitor MP-10 and PDE1 inhibitor DNS-7801. Non-specific binding was determined in the presence of 10 μM PF-05270430 and 100 μM cGMP. The assay solutions were then filtered using Brandel Harvester onto a 96 well GF/C filter plate. After washing and drying the filter plate, each well of the filter was added with 50 mL of Microscint-20 scintillation fluid and the plate counted with a MicroBeta counter (PerkinElmer Life Sciences, Boston, MA, U.S.A.).

Statistical Analysis

Data acquired were analyzed using Prism 7.0 for PC (GraphPad Software Inc., San Diego, CA). All data are presented as mean with S.E.M. The statistical significance was calculated using one-way ANOVA with Bonferroni's post hoc test. The p value of less than 0.05 is defined to be significant. Graphs were plotted using Prism software.

Results

Characterization of K_d and B_{max} of ^{3}H-PF-05270430 with rat brain homogenate and brain sections, binding of PDE2A

PF-05270430 was reported to be highly selective and potent. In a cGMP-stimulated human recombinant full-length PDE2A enzymatic activity assay, its IC_{50} was 0.53 nM

JPET Fast Forward. Published on June 28, 2019 as DOI: 10.1124/jpet.118.255851
This article has not been copyedited and formatted. The final version may differ from this version.

(Zhang et al., 2013). Based on its favorable profile of brain penetration, efflux, and plasma/brain free fraction, the compound was advanced to be labeled with ^{18}F and successfully used in PET imaging study in *cynomolgus (cyno)* monkeys and humans (Zhang et al., 2013, Chen et al., 2016, Naganawa et al., 2016). In the current study, after tritiation, ^{3}H-PF-05270430 maintained its high potency and selectivity. The tracer yielded over 95% specific binding with rat brain homogenate, with K_d of 9.4 nM, 10-20 fold shift comparing with the *in vitro* functional enzymatic activity assay that is commonly seen in other PDEs as well due to the differences of the readout and the enzyme proteins used. The B_{max} values were 1515 fmol/mg (Figure 1A). Incubation of the tracer (10 nM for 1h at room temperature) with rat brain sections demonstrated distinctive PDE2A binding pattern (Figure 1B), consistent with the pattern of PDE2A expression in the brain (Stephenson et al., 2012; Kelly et al. 2013). In the rat brain, high density of PDE2A binding signals were observed in the olfactory bulb, olfactory tubercle, cortex, hippocampus, striatum, ventral tegmental area, as well as the substantia nigra. On coronal sections (data not shown), in the striatum, higher density of binding signals was found in the globus pallidus than in the caudate putamen.

Establishing an exposure occupancy relationship for PF-05180999 at higher dose range

After characterization of the radioligand we established an occupancy dose response for PF-05180999 between the doses of 1 and 150 mg/Kg. A dose-dependent curve was generated against the total plasma concentration of the compound (Figure 2A), with a slope of around 1 and IC_{50} (Occ_{50}) of 965.8 nM total plasma concentration of the

JPET Fast Forward. Published on June 28, 2019 as DOI: 10.1124/jpet.118.255851
This article has not been copyedited and formatted. The final version may differ from this version.

compound. The Occ_{50} value, when back-calculated based on compound's brain penetration, free plasma and free brain percentage, is 122.7 nM, which is largely consistent with *in vitro* Ki assay value (49.0 nM) using rat brain homogenate (Figure 2B). Plasma radioactivity levels at the time when brains were harvested looked constant, no dose-dependent increase or decrease was observed (Figure 2C). However, because each treatment group only had two rats, statistical analysis was not possible.

Efficacy of PF-05180999 in the cFC rat model

To characterize the efficacy of PF-05180999, we choose to perform a model of long-term memory which did not involve the use of chemical impairment. In this case 24h conditioned fear test was utilized. Pre-treatment with oral dose of PF-05180999 at the dose of 0.3 mg/kg prior to training which consisted of 2 0.4mA unconditioned footshocks in the training context produced a significant increase in the rate of freezing behavior 24h later, compared with vehicle-dosed animals. Doses at 0.03 mg/kg or 1 mg/kg were not efficacious, suggesting an inverted U-shaped dose-effect (Fig. 3). Interestingly this dose corresponded well to the previously reported reversal of ketamine working memory impairment reported by Pfizer (Helel, 2018).

***In vivo* PDE2A binding following lower dose range of PF-05180999**

In vivo autoradiography was performed to investigate target engagement by PF-05180999 at the efficacious dose range in the cFC behavior assay. Interestingly,

JPET Fast Forward. Published on June 28, 2019 as DOI: 10.1124/jpet.118.255851
This article has not been copyedited and formatted. The final version may differ from this version.

instead of displacing and thereby decreasing PDE2A tracer binding, lower doses of PF-05180999 appeared to increase the tracer binding and this increase binding tended to return to baseline beyond 3 mg/kg (Figure 4A&B). The increased PDE2A binding does not appear to be the result of increased brain entry of the radioactive tracer, as the plasma radioactivity levels remained constant at the time when the brain samples were harvested (Figure 4C). Total plasma concentration of the drug ranged from 10 nM to 100 nM (Table 1). Since there were only 2-4 rats per group in the first occupancy study and the increase of PDE2A values appeared to be variable, which made one-way ANOVA analysis treacherous, a separate study with increased *n* number per group was performed. PF-05180999 at the p.o. dose of 0.3 mg/kg significantly increased PDE2A tracer binding *in vivo*, compared with the vehicle-control (Figure 5), confirming the results in the previous observation. The dose response was repeated in other 2 separate experiments. The pattern of the PDE2A binding following lower doses of PF-05180999 was established after combining the data of all 4 experiments (Figure 6).

In vitro PDE2A ligand binding in the absence or presence of cGMP

Increased local cGMP levels produced by lower doses of PDE2A inhibitors was suspected to cause the increase in PDE2A tracer binding. To test this hypothesis, *in vitro* PDE2A binding in the presence or absence of various concentrations of cGMP was examined using near-full-length or catalytic-domain recombinant PDE2A protein, or natural PDE2A enzyme in rat brain homogenate. cGMP dose-dependently increased PDE2A tracer binding to the near-full-length PDE2A recombinant enzyme protein - the

activation phase. This facilitation plateaued when cGMP reached 10 to 100 μM. However, when cGMP concentration continued to rise above 100 μM, PDE2A binding decreased in a dose-dependent pattern – the inhibition phase (Figure 7). With catalytic-domain alone, such dual cGMP effect disappeared, only inhibition phase was present (data not shown). Similarly, cGMP also showed dual-phase effect with the natural PDE2A protein in the rat brain homogenate in the presence of 10 μM PDE1 and PDE10 inhibitors. The activation effect plateaued at the concentration of 3 to 16 μM before the inhibition phase kicked in (Figure 8). The cGMP-induced activation of PDE2A binding appeared to be due to the increase of PDE2A affinity. In the presence of fixed concentration of 30 μM cGMP, PDE2A binding curve shifts to the left. Compared with control, K_d value decreased from 17.2 nM to 2.4 nM, an increase of 7.2-fold in affinity (Figure 9).

Discussion

The current study demonstrated that potent and selective PDE2A inhibitor PF-05180999 enhances long-term memory in a contextual fear conditioning model in the rat at the oral dose of 0.3 mg/kg. However, target engagement study using *in vivo* autoradiography failed to show a decrease of PDE2A binding (target occupancy) at this efficacious dose. Instead, a paradoxical, up to 40% increase in PDE2A binding was detected. At higher doses, this compound does decrease PDE2A binding and an occupancy curve against plasma concentration could be generated.

Similar occupancy curve by PF-05180999 has been reported by Chen et al. (Chen et al., 2016) in the *cyno* monkey. Using the same compound PF-05270430 as the tracer (^{18}F-labeled), the authors reported the half maximal effective plasma concentration of 69.4 ng/mL in the region of the striatum (equivalent to 167.5 nm), several fold more potent than that we saw in the rat. This potency mismatch may stem from the differences of species and/or methods used in the experiment and data analysis.

The efficacious dose of the compound in the rat cFC model in the present study overlaps with the dose causing the increase of PDE2A binding capacity. However, It should not assume that memory enhancement effect by PF-05180999 is due to the activation of PDE2A rather than inhibition of the enzyme. Since PF-05180999 compound itself does not directly activate PDE2A, as it failed to increase the binding of the recombinant enzyme in the absence of cGMP at various concentrations (Yan, unpublished data), the increased PDE2A binding capacity appears to be due to the increased level of cGMP – the product of PDE2 enzyme inhibition. Our *in vitro* studies confirmed that cGMP does cause the allosteric modulation of the enzyme itself, as demonstrated by the increase of the tracer binding in both recombinant and natural PDE2A proteins. Increased cGMP at the appropriate levels also activate its downstream kinases and the intracellular cascade and enhances long-term memory in the rat cFC model.

Receptor/target occupancy has been widely used as a platform to explore target engagement for targets such as G-protein-coupled receptors (Yokoi et al., 2002; Kapur et al., 1995; Hargreaves, 2002; Raddad et al., 2016) and transporters (Finnema et al.,

2015; Martin-Facklam et al., 2013) in drug discovery and development. Efforts have been made to demonstrate target occupancy for enzymes (Freedman et al., 2005; Delnomdedieu et al., 2017) as well. One problem for enzyme occupancy studies is, for some enzymes, the cooperativity of the endogenous substrate with the enzyme itself when the compound investigated is the enzyme inhibitor. This cooperativity can change the affinity of the enzyme and significantly change the occupancy-pharmacodynamic relationship as revealed in the present study.

As demonstrated in the present study, the positive cooperativity by increased cGMP is suggested as the reason for PDE2A inhibitor-induced increase in PDE2A binding site availability. The major substrate of PDE2A cGMP not only binds to the catalytic domain, but also allosterically binds, with higher affinity, to the GAF-B domain (Wu et al., 2004), leading to an increased affinity of PDE2A enzyme through conformational changes of the binding pocket in the catalytic subunit (Martin et al., 1982, Pandit et al., 2009). It is our understanding that, under normal circumstances, only a small portion of the PDE2A pool is activated by endogenous cGMP in the rat brain, and thus only a fraction of the high-affinity binding sites is available to the ligand. Inactivated PDE2A enzymes have very low binding affinity. When the animals are dosed with PDE2A inhibitor, increased levels of cGMP will spill over to the adjacent inactive PDE2A pool, opening the active sites to increase the affinity of those enzymes, and cause an increase in the total binding capacity. If at this time there is not enough compound nearby, in quantity or potency or both, an increase of PDE2A binding is observed. This resembles the activation phase that Pandit and colleagues (Pandit et al., 2009) had proposed in the

experiment of investigating ^{3}H-5'-GMP binding in the presence of ascending concentrations of cold cGMP.

Depending on the potency (Ki value) of the compound, the activation phase could be narrow or wide. After testing over 2 dozen orally bioavailable, brain-penetrant PDE2A inhibitors, we found that, except for one compound which has extraordinarily high brain exposure, lower affinity compounds with Ki values higher than 50 nM normally have wide activation phase – they cause an increase of PDE2A binding site availability at the oral doses of 1-100 mg/kg. Higher dose of the compound is needed to fill in the expanded binding capacity for the demonstration of the regular of target occupancy. Conversely, higher affinity compounds with Ki values less than 50 nM can yield a regular dose-dependent PDE2A target occupancy profile at the 1-100 mg/kg dose range, and the negative phase can only be seen in the very low end of the dose range.

The results of our *in vitro* binding studies in the presence or absence of cGMP support the role of cGMP in the activation of PDE2A. These results are consistent with previous PDE2A enzymatic velocity studies (Martins et al., 1982; Pandit et al., 2009). Under *in vivo* conditions, compounds that generate cGMP in the brain via acting on other targets also facilitate PDE2A binding. We (unpublished data) and others (Megens et al., 2017) found that subcutaneous dose of PDE10 inhibitor MP10 could increase *in vivo* PDE2A binding by 3~7-fold. This increase was abolished by pretreatment of L-NAME, a non-selective NO synthase inhibitor that blocks the production of cGMP (Megens et al., 2017). In another study (unpublished data), we found that an *i.p.* dose of ketamine could

JPET Fast Forward. Published on June 28, 2019 as DOI: 10.1124/jpet.118.255851
This article has not been copyedited and formatted. The final version may differ from this version.

also significantly increase *in vivo* PDE2A binding, possibly via ketamine-induced increase of cGMP in the rat brain (Liebenberg et al., 2015).

The activation of PDE2A following enzyme inhibition appears to be consistent with the roles of PDEs. Under physiological states, after the system is activated, the increased intracellular cAMP or cGMP is cleaved by PDEs to allow the system to return to the baseline state and thus get ready for next round of activation. Higher levels of cyclic nucleotide require higher activity of the enzyme, which could be an increase of the binding affinity of the existing enzymes and/or an increase of the total activated forms of the enzymes. This activation may not necessarily be a direct effect on the enzyme such as in PDE2A, it could be indirect, via other intracellular pathways. For example, the activity of PDE1 is dependent on activated Ca^{2+}-calmodulin in the cell (Kakkar et al., 1999). PDE4 inhibition-induced increase of cAMP activates phosphokinase A (PKA), which in turn phosphorylates PDE4. Phosphorylated PDE4 has higher enzymatic activity (Itoh et al., 2010; Song et al., 2016). The direct action of cGMP on PDE2A enzyme protein may be associated with a faster and more efficient activation, indicative of a frontline status of PDE2A in the PDE family (Polito et al., 2013) in coping with increased cGMP in the brain. The reserve of PDE2A appears to be ample as only about 20% of the PDE2A is active under physiological conditions based on the results of *in vivo* activation with PDE10 inhibitor MP-10 (Megens et al., 2017; Gu and Scott, unpublished observation).

It is hard to speculate the kinetics of PDE2A activation following systemic PDE2A inhibitor administration. One of the important reasons is the lack of information of cGMP produced near PDE2A enzyme in the subcellular compartments, although global increase of cGMP was detected after TAK-915 or PF-05180999 administration (Mikami et al., 2017a,b; Helal et al., 2018).

Taken together, similar to the *in vitro* activation and the following inhibition phases in PDE2A binding by ascending concentrations of cGMP (Pandit et al., 2009), PDE2A inhibitor PF-05180999 also triggers activation and inhibition of PDE2A binding *in vivo*, although at lower scales. When evaluating target engagement of PDE2A inhibitors for memory disorder in clinical setting with occupancy assays, the efficacious dose seems unlikely to fall on the typical receptor/target curve. On the contrary, an increase of the tracer binding could be observed. This increase in PDE2A binding in response to PDE2A inhibitor administration could potentially be used to monitor target engagement in clinical development when no other means is available.

Acknowledgements

We thank Dr. Teresa Almos for critical comments on this project, Dr. James DeZazzo for reviewing the manuscript.

Authorship Contributions

Participated in research design: Gu, Scott, Yan, Gomez, Morse, Li, Massari, Breitenbucher, Vivian and Danks

Conducted experiments: Gu, Scott, Yan, Warren and Zhang

Contributed new reagents or analytic tools: Xu, Aertgeerts, Gomez and Breitenbucher

Performed data analysis: Gu, Scott, Yan, Warren, Tabtabaei, Morse and Massari

Wrote or contributed to the writing of the manuscript: Gu, Scott, Yan, Warren, Massari, Breitenbucher and Danks

References

American Psychiatric Association. (2013) *Neurocognitive disorders : Diagnostic and Statistical Manual of Mental Disorders, 5th Eds (DSM-5)*. American Psychiatric Publishing, Arlington, VA.

Boess FG, Hendrix M, van der Staay FJ, Erb C, Schreiber R, van Staveren W, de Vente J, Prickaerts J, Blokland A and Koenig G (2004) Inhibition of phosphodiesterase 2 increases neuronal cGMP, synaptic plasticity and memory performance. *Neuropharmacology* **47**:1081-1092.

Brindle PK and Montminy MR (1992) The CREB family of transcription activators. *Curr Opin Genet Dev* **2**:199-204.

Budson AE and Price BH (2005) Memory dysfunction. *N Engl J Med* **352**:692-699.

Chen G, Zou X, Watanabe H, van Deursen JM and Shen J (2010) CREB binding protein is required for both short-term and long-term memory formation. *J Neurosci* **30**:13066-13077.

Chen L, Nabulsi N, Naganawa M, Zasadny K, Skaddan MB, Zhang L, Najafzadeh S, Lin SF, Helal CJ, Boyden TL, Chang C, Ropchan J, Carson RE, Villalobos A, Huang Y (2016) Preclinical Evaluation of 18F-PF-05270430, a Novel PET Radioligand for the Phosphodiesterase 2A Enzyme. *J Nucl Med* **57**:1448-1453.

Conti M and Beavo J (2007) Biochemistry and physiology of cyclic nucleotide phosphodiesterases: essential components in cyclic nucleotide signaling. *Annu Rev Biochem* **76**:481-511.

Conti M and Richter W (2014) Phosphodiesterases and cyclic nucleotide signaling in the CNS, in Cyclic-Nucleotide Phosphodiesterases in the Central Nervous System (Brandon NJ and West AR eds) pp 1-45, Wiley & Sons, Hoboken, New Jersey.

Delnomdedieu M, Forsberg A, Ogden A, Fazio P, Yu CR, Stenkrona P, Duvvuri S, David W, Al-Tawil N, Vitolo OV, Amini N, Nag S, Halldin C and Varrone A (2017) *In vivo* measurement of PDE10A enzyme occupancy by positron emission tomography (PET) following single oral dose administration of PF-02545920 in healthy male subjects. *Neuropharmacology* **117**:171-181.

Domek-Lopacinska K and Strosznajder JB (2008) The effect of selective inhibition of cyclic GMP hydrolyzing phosphodiesterases 2 and 5 on learning and memory processes and nitric oxide synthase activity in brain during aging. *Brain Res* **1216**:68-77.

Finnema SJ, Halldin C, Bang-Andersen B, Bundgaard C and Farde L (2015) Serotonin transporter occupancy by escitalopram and citalopram in the non-human primate brain: a [(11)C]MADAM PET study. *Psychopharmacology (Berl)* **232**:4159-4167.

Fleischman DA, Wilson RS, Gabrieli JD, Bienias JL and Bennett DA (2004) A longitudinal study of implicit and explicit memory in old persons. *Psychol Aging* **19**:617-625.

Freedman NM, Mishani E, Krausz Y, Weininger J, Lester H, Blaugrund E, Ehrlich D and Chisin R (2005) *In vivo* measurement of brain monoamine oxidase B occupancy by rasagiline, using (11)C-l-deprenyl and PET. *J Nucl Med* **46**:1618-1624.

Ginty DD, Kornhauser JM, Thompson MA, Bading H, Mayo KE, Takahashi JS and Greenberg ME (1993) Regulation of CREB phosphorylation in the suprachiasmatic nucleus by light and a circadian clock. *Science* **260**:238-241.

Gu G, Rojo AA, Zee MC, Yu J and Simerly RB (1996) Hormonal regulation of CREB phosphorylation in the anteroventral periventricular nucleus. *J Neurosci* **16**:3035-3044.

Hargreaves R (2002) Imaging substance P receptors (NK1) in the living human brain using positron emission tomography. *J Clin Psychiatry* **63 Suppl 11**:18-24.

Helal CJ, Arnold E, Boyden T, Chang C, Chappie TA, Fisher E, Hajos M, Harms JF, Hoffman WE, Humphrey JM, Pandit J, Kang Z, Kleiman RJ, Kormos BL, Lee CW, Lu J, Maklad N, McDowell L, McGinnis D, O'Connor RE, O'Donnell CJ, Ogden A, Piotrowski M, Schmidt CJ, Seymour PA, Ueno H, Vansell N, Verhoest PR and Yang EX (2018) Identification of a Potent, Highly Selective, and Brain Penetrant Phosphodiesterase 2A Inhibitor Clinical Candidate. *J Med Chem* **61**:1001-1018.

Itoh T, Abe K, Hong J, Inoue O, Pike VW, Innis RB and Fujita M (2010) Effects of cAMP-dependent protein kinase activator and inhibitor on *in vivo* rolipram binding to phosphodiesterase 4 in conscious rats. *Synapse* **64**:172-176.

Kakkar R, Raju RV and Sharma RK (1999) Calmodulin-dependent cyclic nucleotide phosphodiesterase (PDE1). *Cell Mol Life Sci* **55**:1164-1186.

Kandel ER (2012) The molecular biology of memory: cAMP, PKA, CRE, CREB-1, CREB-2, and CPEB. *Mol Brain* **5**:14.

Kandel ER, Dudai Y and Mayford MR (2014) The molecular and systems biology of memory. *Cell* **157**:163-186.

Kapur S, Remington G, Zipursky RB, Wilson AA and Houle S (1995) The D2 dopamine receptor occupancy of risperidone and its relationship to extrapyramidal symptoms: a PET study. *Life Sci* **57**:PL103-107.

Kelly MP, Adamowicz W, Bove S, Hartman AJ, Mariga A, Pathak G, Reinhart V, Romegialli A and Kleiman RJ (2014) Select 3',5'-cyclic nucleotide phosphodiesterases exhibit altered expression in the aged rodent brain. *Cell Signal* **26**:383-397.

Liebenberg N, Joca S and Wegener G (2015) Nitric oxide involvement in the antidepressant-like effect of ketamine in the Flinders sensitive line rat model of depression. *Acta Neuropsychiatr* **27**:90-96.

Lu Z and Ding L (1999) Blockade of a retinal cGMP-gated channel by polyamines. *J Gen Physiol* **113**:35-43.

Martin-Facklam M, Pizzagalli F, Zhou Y, Ostrowitzki S, Raymont V, Brasic JR, Parkar N, Umbricht D, Dannals RF, Goldwater R and Wong DF (2013) Glycine transporter type 1 occupancy by bitopertin: a positron emission tomography study in healthy volunteers. *Neuropsychopharmacology* **38**:504-512.

Martinez SE, Wu AY, Glavas NA, Tang XB, Turley S, Hol WG and Beavo JA (2002) The two GAF domains in phosphodiesterase 2A have distinct roles in dimerization and in cGMP binding. *Proc Natl Acad Sci U S A* **99**:13260-13265.

Martins TJ, Mumby MC and Beavo JA (1982) Purification and characterization of a cyclic GMP-stimulated cyclic nucleotide phosphodiesterase from bovine tissues. *J Biol Chem* **257**:1973-1979.

Megens AA, Langlois X and Andres-Gil JI (2017) Combinations comprising PDE2A inhibitors such as 1-aryl-4-mehyl-1,2,4 triazolo 4,3-aquinoxaline compounds and PDE10 inhibitors for use in the treatment of neurological or metabloic disorders. *United States* Patent# US9,889,035B2

Mikami S, Kawasaki M, Ikeda S, Negoro N, Nakamura S, Nomura I, Ashizawa T, Kokubo H, Hoffman ID, Zou H, Oki H, Uchiyama N, Hiura Y, Miyamoto M, Itou Y, Nakashima M, Iwashita H, Taniguchi T (2017a) Discovery of a Novel Series of Pyrazolo[1,5-a]pyrimidine-Based Phosphodiesterase 2A Inhibitors Structurally Different from N-((1S)-1-(3-Fluoro-4-(trifluoromethoxy)phenyl)-2-methoxyethyl)-7-methoxy-2-oxo-2,3-dihydropyrido[2,3-b]pyrazine-4(1H)-carboxamide (TAK-915), for the Treatment of Cognitive Disorders. *Chem Pharm Bull (Tokyo)* **65**:1058-1077.

Mikami S, Nakamura S, Ashizawa T, Nomura I, Kawasaki M, Sasaki S, Oki H, Kokubo H, Hoffman ID, Zou H, Uchiyama N, Nakashima K, Kamiguchi N, Imada H, Suzuki N, Iwashita H and Taniguchi T (2017b) Discovery of Clinical Candidate N-((1S)-1-(3-Fluoro-4-(trifluoromethoxy)phenyl)-2-methoxyethyl)-7-methoxy-2-oxo-2 ,3-dihydropyrido[2,3-b]pyrazine-4(1H)-carboxamide (TAK-915): A Highly Potent, Selective, and Brain-Penetrating Phosphodiesterase 2A Inhibitor for the Treatment of Cognitive Disorders. *J Med Chem* **60**:7677-7702.

Montminy MR, Gonzalez GA and Yamamoto KK (1990) Regulation of cAMP-inducible genes by CREB. *Trends Neurosci* **13**:184-188.

Naganawa M, Waterhouse RN, Nabulsi N, Lin SF, Labaree D, Ropchan J, Tarabar S, DeMartinis N, Ogden A, Banerjee A, Huang Y, Carson RE (2016) First-in-Human Assessment of the Novel PDE2A PET Radiotracer 18F-PF-05270430. *J Nucl Med* **57**:1388-1395.

Nakashima M, Imada H, Shiraishi E, Ito Y, Suzuki N, Miyamoto M, Taniguchi T and Iwashita H (2018) Phosphodiesterase 2A Inhibitor TAK-915 Ameliorates Cognitive Impairments and Social Withdrawal in N-Methyl-d-Aspartate Receptor Antagonist-Induced Rat Models of Schizophrenia. *J Pharmacol Exp Ther* **365**:179-188.

Pandit J, Forman MD, Fennell KF, Dillman KS and Menniti FS (2009) Mechanism for the allosteric regulation of phosphodiesterase 2A deduced from the X-ray structure of a near full-length construct. *Proc Natl Acad Sci U S A* **106**:18225-18230.

Paul C, Stratil C, Hofmann F and Kleppisch T (2010) cGMP-dependent protein kinase type I promotes CREB/CRE-mediated gene expression in neurons of the lateral amygdala. *Neurosci Lett* **473**:82-86.

Petersen RC, Smith GE, Waring SC, Ivnik RJ, Tangalos EG and Kokmen E (1999) Mild cognitive impairment: clinical characterization and outcome. *Arch Neurol* **56**:303-308.

Polito M, Klarenbeek J, Jalink K, Paupardin-Tritsch D, Vincent P and Castro LR (2013) The NO/cGMP pathway inhibits transient cAMP signals through the activation of PDE2A in striatal neurons. *Front Cell Neurosci* **7**:211.

Poo MM, Pignatelli M, Ryan TJ, Tonegawa S, Bonhoeffer T, Martin KC, Rudenko A, Tsai LH, Tsien RW, Fishell G, Mullins C, Goncalves JT, Shtrahman M, Johnston ST, Gage FH, Dan Y, Long J, Buzsaki G and Stevens C (2016) What is memory? The present state of the engram. *BMC Biol* **14**:40.

Raddad E, Chappell A, Meyer J, Wilson A, Ruegg CE, Tauscher J, Statnick MA, Barth V, Zhang X and Verfaille SJ (2016) Occupancy of Nociceptin/Orphanin FQ Peptide Receptors by the Antagonist LY2940094 in Rats and Healthy Human Subjects. *Drug Metab Dispos* **44**:1536-1542.

Schmidt CJ (2010) Phosphodiesterase inhibitors as potential cognition enhancing agents. *Curr Top Med Chem* **10**:222-230.

Silva AJ, Kogan JH, Frankland PW and Kida S (1998) CREB and memory. *Annu Rev Neurosci* **21**:127-148.

Soderling TR (1999) The Ca-calmodulin-dependent protein kinase cascade. *Trends Biochem Sci* **24**:232-236.

Song RS, Tolentino R, Sobie EA and Neves-Zaph SR (2016) Cross-regulation of Phosphodiesterase 1 and Phosphodiesterase 2 Activities Controls Dopamine-mediated Striatal alpha-Amino-3-hydroxy-5-methyl-4-isoxazolepropionic Acid (AMPA) Receptor Trafficking. *J Biol Chem* **291**:23257-23267.

Stephenson DT, Coskran TM, Kelly MP, Kleiman RJ, Morton D, O'Neill SM, Schmidt CJ, Weinberg RJ and Menniti FS (2012) The distribution of phosphodiesterase 2A in the rat brain. *Neuroscience* **226**:145-155.

Stroop SD and Beavo JA (1991) Structure and function studies of the cGMP-stimulated phosphodiesterase. *J Biol Chem* **266**:23802-23809.

Teich AF, Nicholls RE, Puzzo D, Fiorito J, Purgatorio R, Fa M and Arancio O (2015) Synaptic therapy in Alzheimer's disease: a CREB-centric approach. *Neurotherapeutics* **12**:29-41.

Tully T, Bourtchouladze R, Scott R and Tallman J (2003) Targeting the CREB pathway for memory enhancers. *Nat Rev Drug Discov* **2**:267-277.

West AE, Chen WG, Dalva MB, Dolmetsch RE, Kornhauser JM, Shaywitz AJ, Takasu MA, Tao X and Greenberg ME (2001) Calcium regulation of neuronal gene expression. *Proc Natl Acad Sci U S A* **98**:11024-11031.

Wu AY, Tang XB, Martinez SE, Ikeda K and Beavo JA (2004) Molecular determinants for cyclic nucleotide binding to the regulatory domains of phosphodiesterase 2A. *J Biol Chem* **279**:37928-37938.

Yokoi F, Grunder G, Biziere K, Stephane M, Dogan AS, Dannals RF, Ravert H, Suri A, Bramer S and Wong DF (2002) Dopamine D2 and D3 receptor occupancy in normal humans treated with the antipsychotic drug aripiprazole (OPC 14597): a study using positron emission tomography and [11C]raclopride. *Neuropsychopharmacology* **27**:248-259.

Legends for Figures

Figure 1: Characterization of PDE2A radiolabeled tracer [^{3}H]PF-05270430 with rat (A) brain homogenate, and the distribution of PDE2A binding with [^{3}H]PF-05270430 on sagittal rat (C) brain sections. Specific binding exceeded over 95% in the rat (A and B), and distinctive binding signals (red, yellow, and green) was observed in the rat brain sections (C and D). CP, caudate putamen; GP, globus pallidus; Hippo, hippocampus; OT, olfactory tubercle; PFC, prefrontal cortex; SN, substantia nigra.

Figure 2: PDE2A occupancy following higher oral dose range (1-150 mg/kg) of PF-05180999, plotted against total plasma concentration of the drug (A). PDE2A target occupancy plotted against the calculated free brain concentration (dot) is consistent with the result of *in vitro* displacement (Ki) assay(triangle) (B). PF-05180999 does not appear to impact radioactivity levels in the plasma 10 min after 1 μCi/g in injection of the tracer when the brain samples were harvest, as a dose-dependent increase or decrease by the compound could not be established (n = 2) (C).

Figure 3: PF-05180999 enhances long-term memory in contextual fear conditioning model in the rat. Mean percentage freezing (±SEM) during the 3 min contextual fear memory test. PF-05180999 dosed at 0.3 mg/kg enhanced long-term contextual fear memory compared to the vehicle-treated 2US control rats. Rats (n=32/group) were dosed (p.o., 2 mL/kg, vehicle =10:40:50 NMP:PEG400:H2O or PF05180999) 60 min prior to training (which consisted of 2 0.4mA footshocks in the training context).

Contextual fear memory was tested 24h after training. Asterisk = $p < 0.05$ vs. 2US vehicle (ANOVA, least means square post hoc comparison).

Figure 4: PDE2A target binding following lower oral range (0.03-3 mg/kg) of PF-05180999 in the rat. PF-05180999 significantly increased PDE2A tracer binding at the dose of 0.3 mg/kg and the binding intensity tended to be returning to baseline when the doses of the drug were increased (n = 3 per group) (A and B). Plasma radioactivity levels remained constant 10 min after 0.5 μCi/g *i.v*. injection of the tracer right before the brain samples were harvested (C).

Figure 5: Comparison of PDE2A tracer binding between vehicle- or PF-05180999 (0.3 mg/kg, p.o., 1h postdosing)-treated groups. PF-05180999 significantly increases the binding. n = 7 in the vehicle group and n = 8 in the drug treatment group.

Figure 6: Increase of PDE2A tracer binding over vehicle treatment after lower dose range (0.03-10 mg/kg) of PF-05180999 – data combining the results of 4 separate experiments. (0.03 mg/kg, n = 6; 0.1 mg/kg, n = 3; 0.3 mg/kg, n = 17; 1 mg/kg, n = 9; 3 mg/kg, n = 6; 10 mg/kg, n = 3). PF-05180999 at the doses of 0.1, 0.3, 1, and 3 mg/kg increases the binding of PDE2A tracer [^{3}H]PF-05270430. This increase tends to return to baseline when the dose of the compound is beyond 3 mg/kg.

Figure 7 *In vitro* PDE2A tracer ^{3}H-PF-05270430 binding with recombinant PDE2A (215-900) protein in the absence or presence of ascending cGMP. PDE2A binding increases with initial ascending concentrations of cGMP then plateaus and finally decreases when cGMP concentration becomes higher.

Figure 8: *In vitro* PDE2A tracer ^{3}H-PF-05270430 binding with rat brain homogenate that contains native PDE2A protein in the absence or presence of ascending cGMP. Similar to Figure 6 that uses PDE2A (215-900) protein, PDE2A binding increases with initial ascending concentrations of cGMP then plateaus and finally decreases when cGMP concentration becomes higher.

Figure 9: *In vitro* PDE2A tracer ^{3}H-PF-05270430 binding with recombinant near-to-full length PDE2A protein in the absence or presence of 30 μM cGMP. The binding saturation curve shifts to the left in the presence of 30 μM cGMP, comparing with curve treated with buffer alone. Activated PDE2A has over 7-fold higher affinity over the inactive form.

Tables

Table 1. Plasma drug concentration following low doses of PF-05180999 p.o. dosing

PF-05180999 (mg/kg, p.o.)	[Total Plasma] (nM)
0.03	BQL
0.3	14.2
1	38.2
3	110.0

JPET Fast Forward. Published on June 28, 2019 as DOI: 10.1124/jpet.118.255851
This article has not been copyedited and formatted. The final version may differ from this version.

Figures

Figure 1

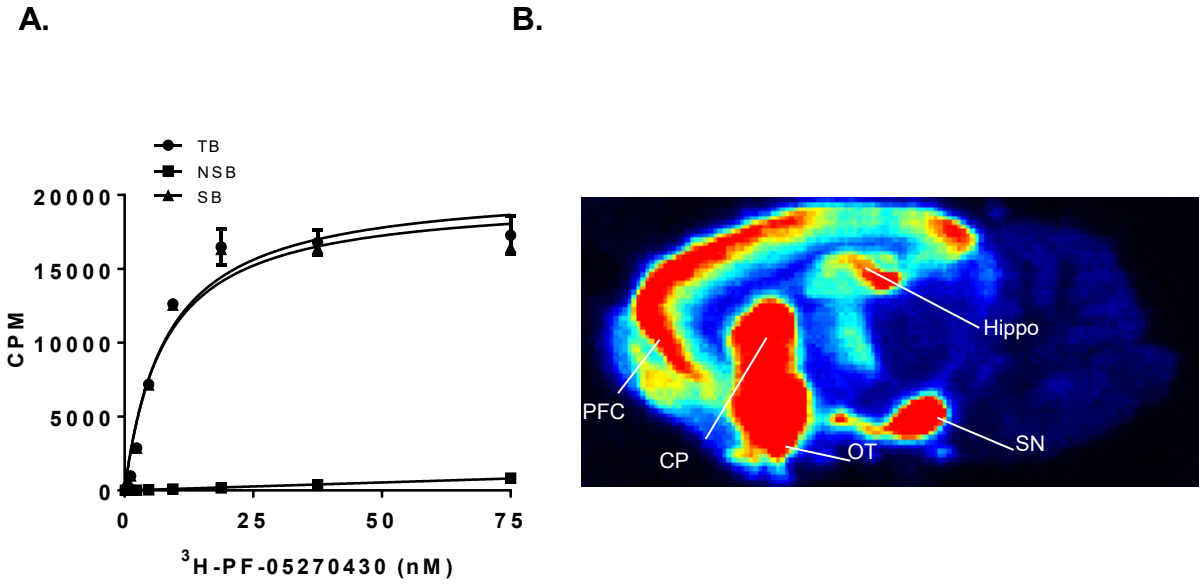

JPET Fast Forward. Published on June 28, 2019 as DOI: 10.1124/jpet.118.255851
This article has not been copyedited and formatted. The final version may differ from this version.

Figure 2

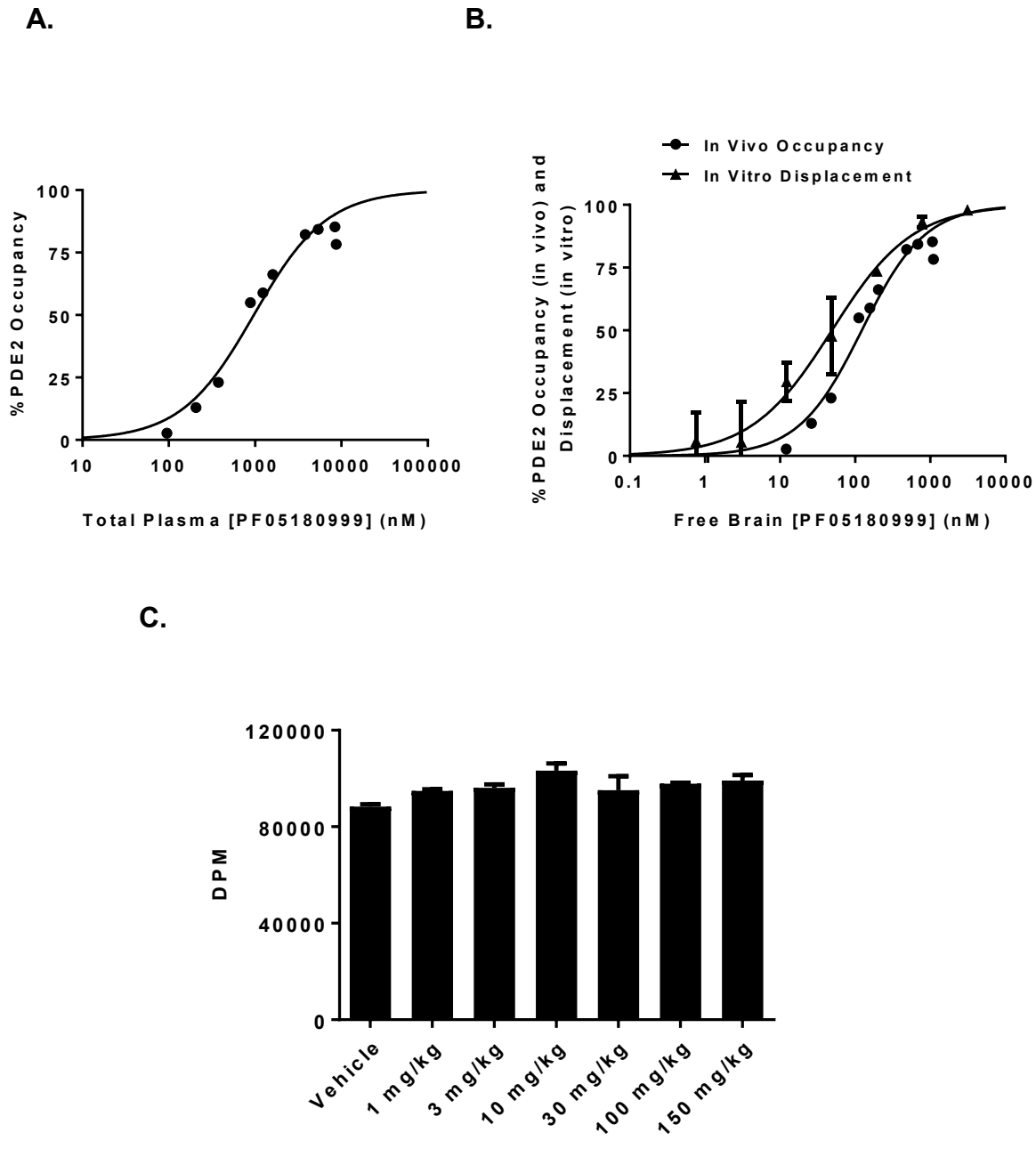

JPET Fast Forward. Published on June 28, 2019 as DOI: 10.1124/jpet.118.255851
This article has not been copyedited and formatted. The final version may differ from this version.

Figure 3

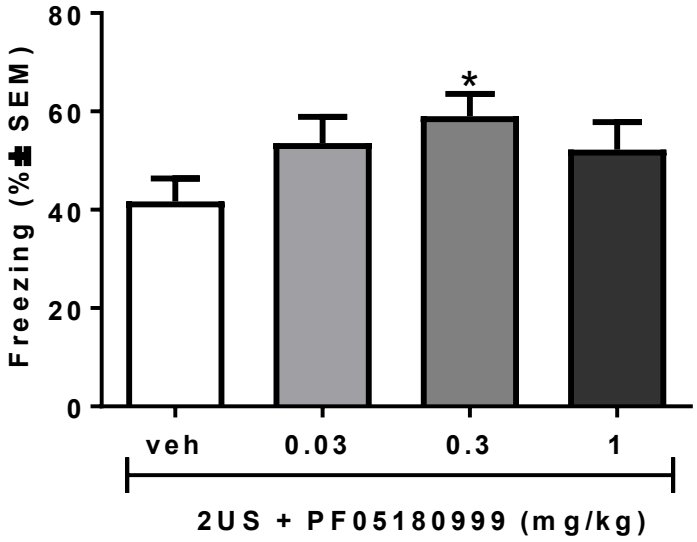

JPET Fast Forward. Published on June 28, 2019 as DOI: 10.1124/jpet.118.255851
This article has not been copyedited and formatted. The final version may differ from this version.

Figure 4

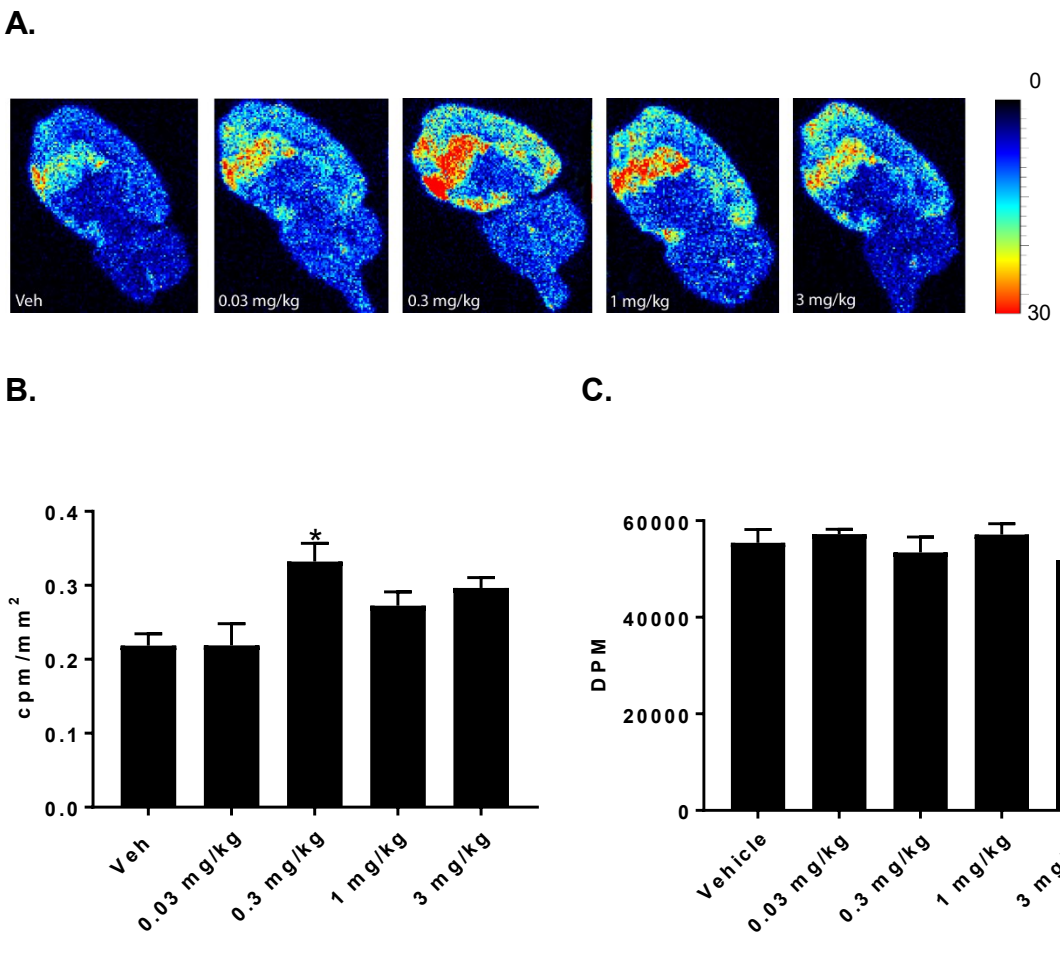

JPET Fast Forward. Published on June 28, 2019 as DOI: 10.1124/jpet.118.255851
This article has not been copyedited and formatted. The final version may differ from this version.

Figure 5

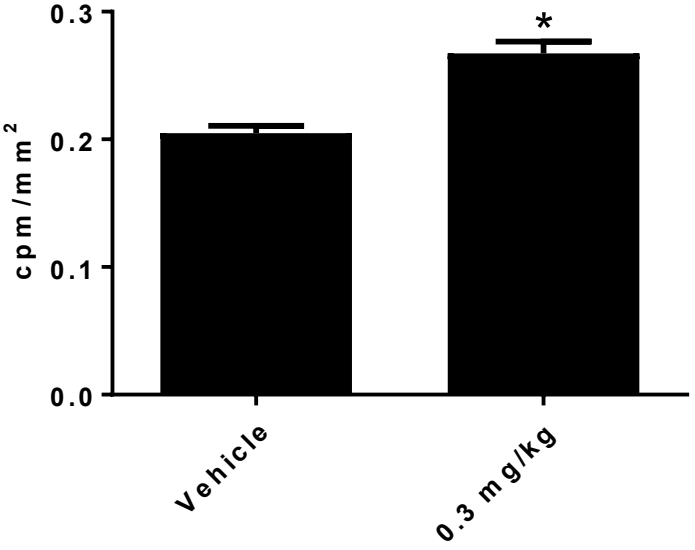

Figure 6

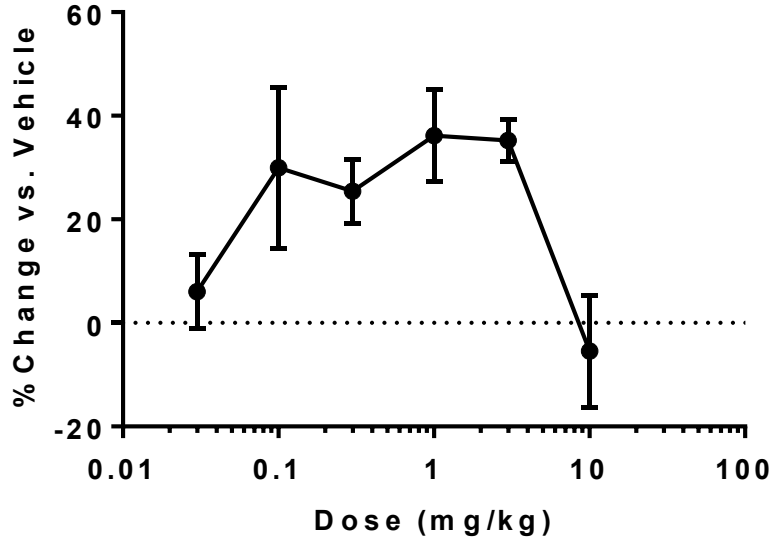

JPET Fast Forward. Published on June 28, 2019 as DOI: 10.1124/jpet.118.255851
This article has not been copyedited and formatted. The final version may differ from this version.

Figure 7

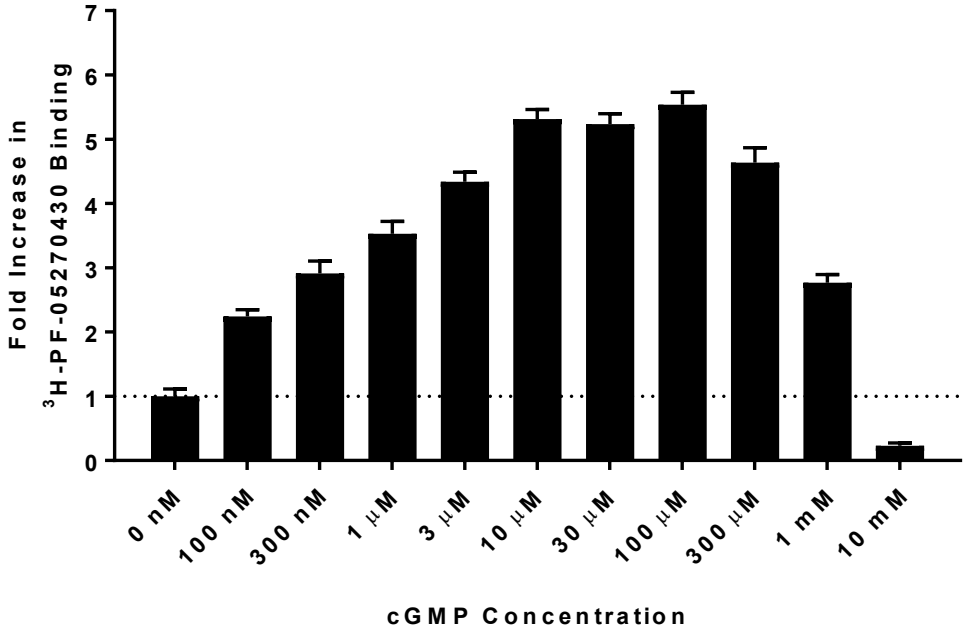

Figure 8

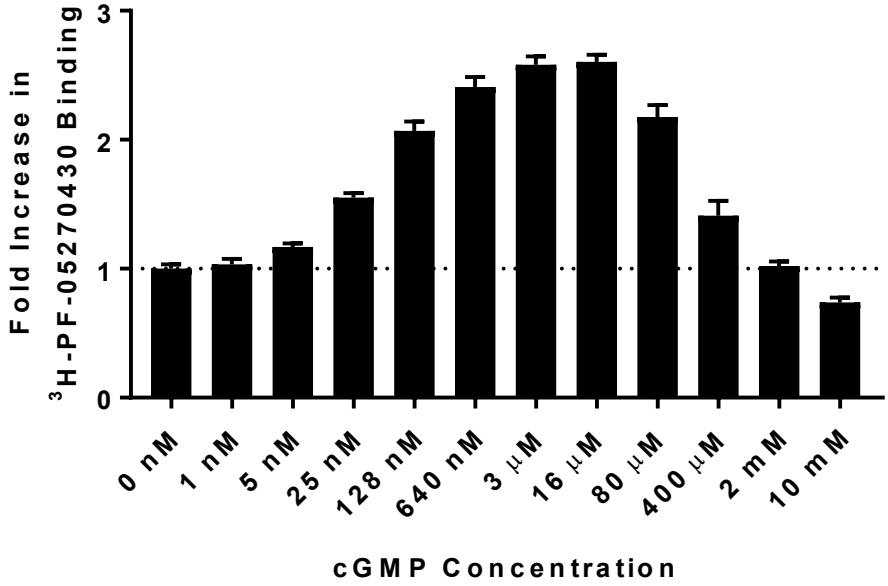

JPET Fast Forward. Published on June 28, 2019 as DOI: 10.1124/jpet.118.255851
This article has not been copyedited and formatted. The final version may differ from this version.

Figure 9